Depth-Profiling Analysis of Multilayer Samples with Two-Dimensional Fourier Transform Infrared Multiple-Angle Attenuated Total Reflection Spectroscopy

Nishikawa, Yuji*

Depth-profiling analysis of multilayer samples with a generalized two-dimensional (G2D) correlation technique equipped with a multiple-angle single-reflection attenuated total reflection (s-ATR) spectroscopy has been reported. ATR spectra at different incident angles are used to generate two-dimensional (2D) correlation spectra. The relative spatial interactions of correlated signals are then determined from the signs of the corresponding contours of the asynchronous correlation map. To apply this method to multilayer samples, effects of dispersion in refractive indices of materials which create pseudo-contours were first investigated with simulated ATR spectra. A 0.1 μm thick gelatin layer on a polyester film and a 0.2 μm thick polycarbonate layer on the gelatin/polyester film were investigated as actual model samples. These layers were thin, but relative depths of each layers were clearly distinguished.

1 INTRODUCTION

The depth-dependent composition changes in a polymer film can arise from various conditions including processing environment, temperature, and surface treatment. As a result of the treatments, film compositions are not constant, especially in the depth direction. Since the actual macroscopic properties of polymeric films, such as adhesion and degradation, are largely affected by the concentration changes across the film, the depth characterization of the compositions is essential.

One of the most useful and well-known techniques for the characterization of polymer films is Fourier transform infrared attenuated total reflection (FT-IR/ ATR) spectroscopy. Since the development of the technique by Harrick[1,2] and Fahrenfort,[3] it has found a great number of applications including surface characterization[4-9] and depth profiling of polymer films.[10-15]

Recently, depth profiling by multiple-angle FT-IR/ ATR spectroscopy has been extensively applied. The depth profiling information via multiple-angle FT-IR/ ATR spectroscopy can be obtained either by the inverse Laplace transformation[10-14] or by exact optical theory.[15-17] The former method, however, is limited to bands with small absorption coefficients, because of the difficulty of numerical inversion of Laplace transformation due to the so-called ill-conditioned problem.[15,16] Because most absorption coefficients of main (or fingerprint) absorptions in polymeric films are not weak, the inverse Laplace transform method is not always available. The application of exact optical theory is not limited by the magnitude of the absorption coefficient; however, its process is mathematically complex and is limited to two-component systems. Theoretically, this method is applicable to more than two-component systems, but a large number of unknowns in the combined equation set make it difficult to determine the depth profile.[15]

Another approach is Fourier transform infrared photoacoustic (FT-IR/PAS) depth-profiling analysis.[18-22] In this method of depth-profiling analysis, variation of the modulation frequency or analysis of the phase angle, or both, may be used. Two-dimensional (2D) correlation can be also be applied to PAS depth-profiling analysis.[19-21] Depth resolu-tion on the order of 1 μm has been demonstrated by use of FT-IR/PAS.[22]

Since the probing depth of FT-IR/ATR is on the order of 0.2 to 3 μm, its combination with 2D analysis has the potential for determining a structure with depth resolution of 1.0 μm or less. In the present paper, we report a new application of generalized two-dimensional (G2D) correlation spectroscopy in FT-IR/ATR depth-profiling analysis. Multiple-angle FT-IR/ATR spectra of multilayer samples are used to calculate G2D correlation maps. Advantages and limitations of this analysis method in enhancing spectral as well as depth resolutions will be discussed.

2 THEORY

In ATR spectral depth-profiling analysis, the refractive indices of ATR crystals and incident angle variations can be regarded as external perturbations. In ATR spectroscopy, the penetration depth (d_p) from sample surfaces is defined as the following equation:

$$d_p = \frac{\lambda}{2\pi n_0}\left[\sin^2\alpha - \left(\frac{n_1}{n_0}\right)^2\right]^{-1/2} \quad (1)$$

* Central Research Laboratory

where λ is the wavelength of the incident beam, and n_0 and n_1, are the refractive indices of the ATR crystal and sample, respectively. As shown in the equation, the penetration depth at any specific wavelength λ is strongly affected by the incident angles and the refractive indices of the ATR crystals. Thus, this perturbation will cause spectral intensity variations, with surface signals appearing relatively stronger than bulk signals when lower penetration depths are chosen, and vice versa. Therefore, the G2D correlation analysis can be adapted to the multiple-angle ATR spectral data. Given a penetration depth (d_p), induced spectral-intensity variation $\tilde{y}(\bar{\nu}),d_p$ at wavenumber observed over an incident angle range (or refractive index range) F, the synchronous and asynchronous correlation intensities between $\bar{\nu}_1$, and $\bar{\nu}_2$ are defined by

$$\Phi(\bar{\nu}_1,\bar{\nu}_2)+i\Psi(\bar{\nu}_1,\bar{\nu}_2)=\frac{1}{\pi F}\int_0^\infty \tilde{Y}_1(\omega)\,\tilde{Y}_2{}^*(\omega)\,d\omega \quad (2)$$

where $\tilde{Y}_1(\omega)$ is the incident angle-domain Fourier transform of $\tilde{y}(\bar{\nu}_1,d_p)$, and $\tilde{Y}_2^*(\omega)$ is the conjugate of the Fourier transform of $\tilde{y}(\bar{\nu}_2,d_p)$ with a Fourier frequency of ω. Thus, the G2D correlation spectra can be obtained from any penetration depth-dependent spectra, as long as the Fourier transform of the incident angle dependence can be calculated for the intensity changes at each wavenumber.

G2D/ATR correlation spectra can be calculated from a series of one-dimensional spectra collected at different penetration depths. In FT-IR/ATR, these spectra can be collected from different incident angles by using the same ATR crystal in multiple-angle ATR mode. The multiple-angle ATR experiment is easily achieved by using variable-angle internal single-reflection optics equipped with a hemicylinder-shaped crystal.

3 EXPERIMENTAL

FT-IR/ATR spectra were recorded on a Nicolet Magna 860 spectrometer equipped with a Harrick multiple-angle single-reflection ATR accessory, which allows the external angles of incidence to be continuously varied from 35° to 75°, and with a DTGS detector, for 256 scans per spectrum at 4 cm^{-1} resolution under purged N_2 gas. In order to obtain various penetration depths, the following two crystals were used: a ZnSe hemicylinder of 7.5 mm in radius and a germanium hemicylinder of the same radius. The incident light was polarized perpendicular to the plane of reflection.

A series of ATR spectra, arranged from lower incident angles to higher ones, were then converted to text formats (#.csv) and loaded into a Mathematica program routine. G2D correlation intensity data were calculated by using Mathematica Version 4.0 for Windows 98. The Mathematica G2D correlation program was created in accordance with Noda's Fourier transform theory[21] and generated as contour maps. Since these data sets are all positive and the ATR signal intensity decreases as penetration depths decrease, all G2D/ATR synchronous contours must be positive according to the G2D theory.[23]As described in the G2D photoacoustic analysis,18 this significant feature also simplifies the G2D/ATR analysis rules.
The samples used in these experiments included a single-layer sample, amorphous polyester film; a two-layer sample, 0.1 μm gelatin on the polyester film (Gel/PES); and a three-layer sample, 0.2 μm polycarbonate (PC) on 0.1 μm gelatin on the PES film (PC/Gel/PES). The PES thickness is about 100 μm.

4 RESULTS AND DISCUSSION

4.1 Simulation Study.

As indicated by Jiang and Palmer,[19] extreme caution must be taken in analyzing high-resolution 2D correlation peaks, particularly in the asynchronous correlation spectra, since in some cases artifacts may appear. In the G2D ATR correlation analysis, possible artificial peaks may occur due to dispersion in the refractive indices of materials which cannot be attributed to chemical, physical (crystallinity or orientation), or spatial properties of the samples. In the present paper, in order to determine the effects of dispersion in refractive indices of materials in G2D asynchronous correlation peaks, simulated ATR spectra were synthesized first, and the effects, particularly in the asynchronous correlation spectra, were examined with the use of their simulated ATR spectra.

The ATR spectra can be synthesized by use of model optical constants according to Fresnel's equation for perpendicular light polarization,

$$R=\frac{w^2+Y-2wa}{w^2+Y+2wa} \quad (3)$$

$$w=n_0\cos\alpha \qquad \alpha=\left(\frac{Y+X}{2}\right)^{1/2}$$

$$X=n^2-k^2-n_0^2\sin^2\alpha \quad (4)$$

$$Y=\left(X^2+4n^2k^2\right)^{1/2} \quad (5)$$

where n_0 is the refractive index of the ATR crystal, and α is the angle of incidence. The model absorption spectrum can be generated from antisymmetric linear combinations of the Lorentzian functions:[24-25]

$$k=\frac{k_{\max}\gamma^2}{(\bar{\nu}-\bar{\nu}_0)^2+\gamma^2}-\frac{k_{\max}\gamma^2}{(\bar{\nu}-\bar{\nu}_0)^2+\gamma^2} \quad (6)$$

In the mid-IR range, k in Eq. 6 is dominated by the first term, representing a Lorentzian band with a maximum k_{Max} at ν_0 and a half-width at half-

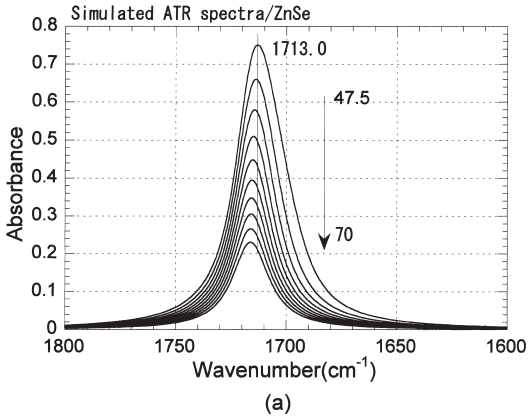

Fig.1a. A set of simulated FT-IR/ATR spectra of C=O bands, n_0 = 1722 cm^{-1}; k_{max} = 0.54; g = 10 cm^{-1}; α = 47.5 to 70°, 2.5° increments; n_0 = 2.40 (for ZnSe); n_∞ = 1.570.

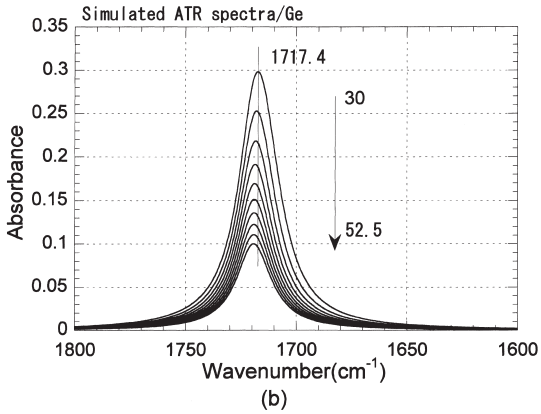

Fig.1b. A set of simulated FT-IR/ATR spectra of C=O bands, α = 30 to 52.5°, 2.5° increments; n_0 = 4.00 (for Ge); $n\infty$ = 1.570.

maximum (HWHM) equal to γ. The presence of the second term in Eq. 6 makes it possible to calculate the corresponding refractive index spectrum accord- ing to the following equation:[22-23]

$$k = n_\infty - \frac{(\bar{\nu}-\bar{\nu_0})k_{max}\gamma}{(\bar{\nu}-\bar{\nu_0})^2+\gamma^2} - \frac{(\bar{\nu}+\bar{\nu_0})k_{max}\gamma}{(\bar{\nu}+\bar{\nu_0})^2+\gamma^2} \quad (7)$$

where n_∞ represents the assumed refractive index at infinite wavenumber.

In an effort to simulate C=O bands of a polyester film, a series of spectra containing 107 data points was generated in the spectral range from 1800 to 1600 cm^{-1} with = 1722 cm^{-1}; k_{max} = 0.54; γ = 10 cm^{-1}; α = 47.5 to 70° for n_0 = 2.40 (ZnSe), and α = 30 to 52.5° for n_0 = 4.00 (Ge); and n_∞ = 1.570. These simulated spectra and their G2D asynchronous correlation contour maps are shown in Figs. 1 and 2. Figures Ia and Ib show series of simulated ATR spectra with various incident angles of 47.5 to 70° for ZnSe (n_0 = 2.40), and with incident angles of 30 to 52.5° for Ge (n_0 = 4.00), respectively. Figures 2a and 2b show the contour maps obtained from the asynchronous correlation analysis of Figs. 1a and 1b, respectively. The shaded area represents a negative intensity region.

As expected, significant artificial contours were generated in the asynchronous correlation maps. In the case of ZnSe crystal, shown in Fig. Ia, a maximum peak location at an incident angle of 47.5° was observed at 1713.0 cm^{-1}, and the peak location shifted to 1716.2 cm^{-1} with increasing incident angle to 70.0°. This peak shift is caused by dispersion in the refractive index of the simulated sample.26 In other words, decreases of peak intensities in the regions lower than 1714.6 cm^{-1} ($\bar{\nu_1}$) in wavenumber are faster than those in the regions larger than 1714.6 cm^{-1} ($\bar{\nu_2}$), with increasing the incident angles. As a result, shown in Fig.2a, in the asynchronous correlation contours, the spectral regions lower than 1714.6 cm^{-1} show positive correlation with the spectral regions higher than that frequency, while the regions larger than 1714.6 cm^{-1} negatively correlate with the lower regions.

This positive-negative contour is a consistent finding for the rules originally proposed by Noda for

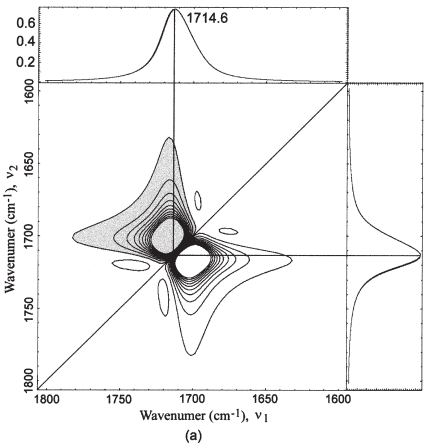

Fig.2a. Simulated asynchronous 2D ATR correlation contour maps of C=O bands generated from (a) simulated spectra shown in Fig. Ia. The shaded area represents a negative intensity region.

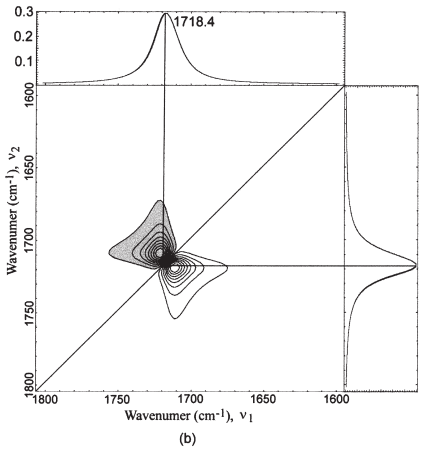

Fig.2b. Simulated asynchronous 2D ATR correlation contour maps of C=O bands generated from (a) simulated spectra shown and (b) in Fig. Ib. The shaded area represents a negative intensity region.

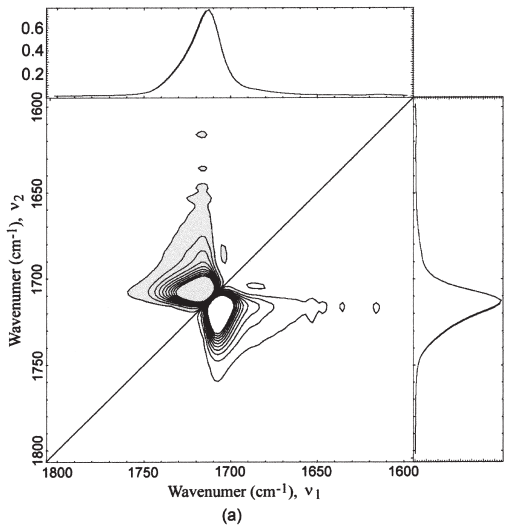

Fig.3a. Actual asynchronous 2D ATR correlation contour maps of polyester C=O bands, a ZnSe ATR crystal; incident angle range = 47.5 to 70°; 2.5° in increments. The shaded area represents a negative intensity region.

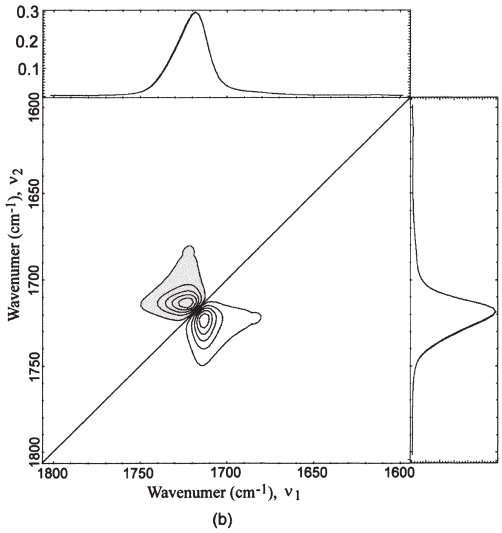

Fig.3b. Actual asynchronous 2D ATR correlation contour maps of polyester C=O bands, a Ge ATR crystal; incident angle range = 30 to 52.5°; 2.5° increments. The shaded area represents a negative intensity region.

the analysis of 2D correlation maps.23 In addition, when the positive-negative contour map was folded along a diagonal line, the two contour patterns were completely matched except for their positive or negative sign. The presence of these positive- negative contours closely arranged around a diagonal area and their line symmetrical features can be regarded as evidence of artificial creations due to dispersion in refractive indices of samples in 2D ATR.

In the case of the Ge crystal. Fig. 1b, a maximum peak location at an incident angle of 30° was observed at 1717.4 cm^{-1}, and the peak location shifted to 1719.4 cm^{-1} with increasing incident angle to 52.5°. The magnitude of peak shift with the use of the Ge crystal is 2 cm^{-1} which is smaller than that with the ZnSe crystal (3.2cm^{-1}). The resulting asynchronous correlation map also shows positive-negative contours that are the same as those with the use of the ZnSe crystal; however, absolute asyn- chronous correlation intensities (less than 0.01) and the contour area around diagonal positions at 1718.4cm^{-1} are weaker than those with the ZnSe crystal, as shown in Figs. 2a and 2b.

Figures 3a and 3b show the actual asynchronous correlation contour maps of the C=O bands of PES films obtained from the use of ZnSe and Ge crystals, respectively. Although minor differences between the correlation patterns of these maps and the simulated patterns are seen, similar symmetrical positive-negative line contours are clearly observed. In addition, the artifactual correlation intensity of the C=O band with the use of the ZnSe crystal is larger than that for the Ge crystal, similar to that observed in the simulated results, suggesting that the use of the Ge crystal is preferable to the ZnSe crystal because of its minimum artificial creations.

These positive-negative contour patterns observed around diagonal area in asynchronous correlation contours in 2D/ATR spectra should be excluded as pseudo-contours that can not be attributed to chemical, physical, and/or spatial interactions of samples.

4 G2D Analysis of Multilayer Films.

We have attempted depth-profiling analysis of two- and three-layered films based on the above basic study. Figure 4 shows an asynchronous correlation contour map of the 0.1 μm Gel/PES film. Since synchronous correlation contours of the Gel/PES film were all positive, we have analyzed asynchronous correlation contours only. The positive-negative contour bands at 1717cm^{-1}, which are in close proximity to each other at the diagonal position, can be attributed to the dispersion in refractive indices of the PES film. The positive- negative contour bands at 1602/1717 and 1502/1717cm^{-1} in the off-diagonal area can also be attributed to the dispersion in refractive indices of the PES film. Since both 1602 and 1502 c m^{-1} bands are weak (k = 0.15 or less), positive-negative contours at the diagonal position were not observed. In the simulated results, the dispersion effects are found to be observed as positive-negative contours which are in close proximity to each other around both diagonal and off-diagonal area in asynchronous contour maps. When these positive-negative contours are observed in any area, they should be considered as evidence of dispersion effects and excluded for the data analysis.

Only negatively correlated contours were seen between the 1645 and 1540cm^{-1} (ν_1) bands, which are

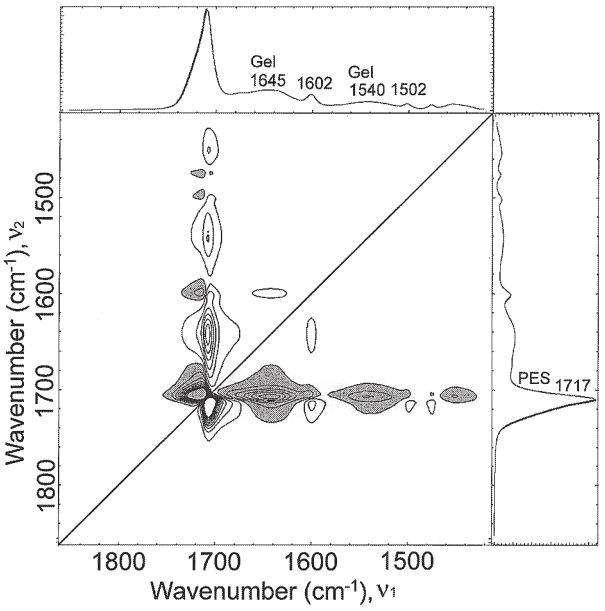

Fig. 4. Asynchronous 2D ATR correlation contour maps of 0.1 μm thick gelatin layer on polyester (Gel/PES): Ge ATR crystal; incident angle range = 30 to 52.5°; 2.5° increments. Both positive and negative contours are shown. The shaded area represents a negative intensity region.

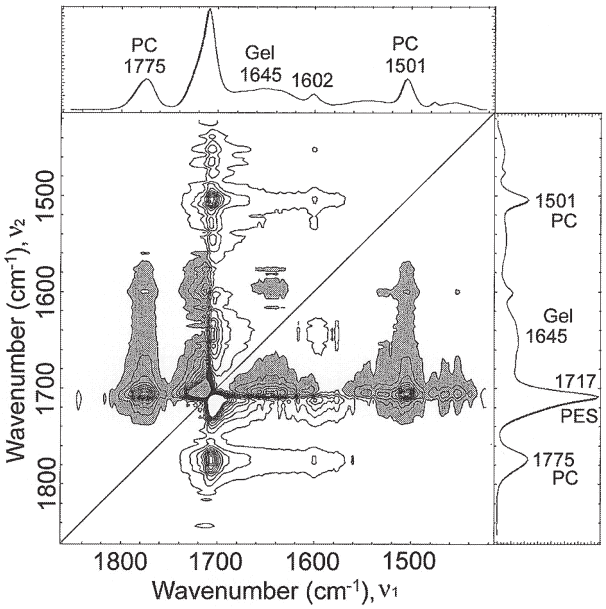

Fig. 5. Asynchronous 2D ATR correlation contour maps of 0.2 μm thick polycarbonate layer on 0.1 μm thick gelatin layer on polyester (PC/Gel/PES): Ge ATR crystal; incident angle range = 30 to 52.5°; 2.5° increments. Both positive and negative contours are shown. The shaded area represents a negative intensity region.

attributed to the amide I and II bands of the Gel layer, and the 1717cm^{-1} band (ν_2) of PES film, indicating that the decrease in these bands with decreasing the ATR penetration depth is slower than that of 1717cm^{-1}. This result indicates that the Gel layer is closer to the surface than the PES film. The absence of the positive-negative contours in the off-diagonal area indicates that the correlation intensity between the two Gel bands and the 1717 cm^{-1} PES band due to dispersion is negligibly weaker than that produced by the special interaction between the Gel and PES layer.

An asynchronous correlation contour map of the three-layer film (0.2 μm PC/0.1 μm Gel/PES) is shown in **Fig. 5**. Although a more complex contour map was obtained compared to that of the two-layer system, the order of each layers of the sample can be obviously identified from the signs of the asynchronous correlation contours shown in the figure. Similar positive-negative contours were again observed near the diagonal position of 1717cm^{-1} and in the off-diagonal area of 1602/ 1717cm^{-1} attributed to the dispersion effect of the PES. The negative contours at 1775/1705, 1775/1645, 1501/1705, and 1501/1645cm^{-1} (ν_1/ν_2) show that the origins of the bands at 1775 and 1501cm^{-1} (PC) are shallower thanthose of 1705 (PES) and 1645cm^{-1} (Gel). The negative contour at 1645/1705cm^{-1} and the positive contours at 1645/ 1775 and 1645/1501cm^{-1} show that the origin of the band at 1645cm^{-1} (Gel) is shallower than that of 1705cm^{-1} (PES) but deeper than those of 1775 and 1501cm^{-1} (PC). Similarly, it can be determined that the origin of the PES band (1705 cm^{-1}) is deeper than those of the GEL band (1645 cm^{-1}) and PC band (1775cm^{-1}). Thus, the order of layers of this sample, as determined from multiple-angle ATR spectral depth profiling, is PC, Gel, and PES from top to bottom, in agreement with the known structure. Although the thickness of the Gel layer is thin (0.1 μm), the depth interaction between the Gel, PC, and PES can be unambiguously determined, indicating that the depth resolution of the present method is much higher than has been demonstrated by FT-IR/PAS spectral depth-profiling analysis.

5 CONCLUSION

G2D FT-IR/ATR correlation spectroscopy and its applications to depth-profiling analysis of multilayer samples have been described and demonstrated in the present paper. With this method, ATR spectra at different incident angles (i.e., the external perturbation) are used to generate 2D correlation spectra, and the signs of correlation contours provide enough information to determine the spatial (depth) relation of correlated signals. This method provides improved depth resolution, since generalized 2D correlation analysis reveals spatial origin-related spectral details, which are usually obscured in a one-dimensional spectrum. In this experiment, the relative depth of a 0.1 μm thick Gel layer can be obviouly identified.

In ATR spectroscopy, the spatial resolution may be significantly higher near the surface (may be larger than 0.1 μm), since the signal-to-noise ratio is very high for species near the surface due to the exponential decay profile of the mean square electric

field. However, deeper into the sample the signal-to-noise ratio from those components suffers due to the small electric field intensity at those depths. The resolution should be degraded by this low signal. On the basis of the present data, the spatial resolution, from the surface to about 3 μm in depth, may be 0.1 μm or less with the use of a Ge ATR crystal. Further investigations should be performed to confirm the overall spatial resolutions in G2D ATR analysis for all cases.

In the present method, however, the following limitation has been revealed: this approach creates artificial contours, especially in asynchronous correlation analysis, which cannot be attributed to chemical, physical, or spatial interactions of samples. These pseudo-contours are mainly due to dispersion in the refractive indices of the samples and are strongly associated with the refractive indices of the ATR crystals used. In the actual multilayer samples, when a Ge crystal was used, the pseudo-contours were almost negligible, as shown in Figs.6 and 7. When one is using other crystals that have lower refractive indices, including ZnSe, KRS-5, and diamond, or in combination with the multi-crystal ATR mode, the pseudo-contours cannot be neglected. If the removal of these effects can be attained by the use of several approaches (e.g., exact optical theory), the present method will be more widely applicable. Further continuous investigation, qualitatively and quantitatively, should be performed to solve these problems.

This paper is a partial copy of a paper entitled "Generalized Two-Dimensional Fourier Transform Infrared Multiple-Angle Attenuated Total Reflection Spectral Depth-Profiling Analysis of Multilayer Samples", which is published in Applied Spectroscopy, 53, 9,1054 (1999), with permission of the Society for Applied Spectroscopy.

6 REFERENCES

1. N. J. Harrick, Phys. Rev. Lett. **4,** 244 (1960).
2. N. J. Harrick, J. Phys. Chem. **64,** 1110 (1960).
3. J. Fahrenfort, Spectrochim. Acta **17,** 698 (1961).
4. C. S. Blackwell. P. J. Degen, and E. D. Osterholtz, Appl. Spectrosc. **32,** 480 (1978).
5. P. A. Temple, Appl. Opt. **20,** 2657 (1981).
6. R. Iwamoto and K. Ohta, Appl. Spectrosc. **38,** 359 (1984).
7. Y. Ishino and H. Ishida, Appl. Spectrosc. **42,** 1296 (1988).
8. C. G. L. Khoo and H. Ishida, Appl. Spectrosc. **44,** 512 (1990).
9. Y. Ishino and H. Ishida, Appl. Spectrosc. **46,** 504 (1992).
10. K. Ohta and R. Iwamoto, Appl. Spectrosc. **30,** 418 (1985).
11. L. J. Fina and G. Chen, Vib. Spectrosc. **1,** 353 (1991).
12. M. Yanagimachi, M. Toriumi, and H. Masuhara, Appl. Spectrosc. **46,** 832 (1992).
13. R. A. Shick, J. L. Koenig, and H. Ishida, Appl. Spectrosc. **47,** 1237 (1993).
14. H. Ishida, Bull. Inst. Chem. Res., Kyoto Univ. **71,** 190 (1993).
15. J. Huag and M. W. Urban, Appl. Spectrosc. **47,** 973 (1993).
16. S. Ekgasit and H. Ishida, Appl. Spectrosc. **50,** 1187 (1996).
17. S. Ekgasit and H. Ishida, Appl. Spectrosc. **51,** 1488 (1997).
18. E. Y. Jiang, W. J. McCarthy, D. L. Drapcho, and R. A. Crocombe, Appl. Spectrosc. **51,** 1736 (1997).
19. E. Y. Jiang and R. A. Palmer, Anal. Chem. **69,** 1931 (1997).
20. R. A. Palmer, Spectroscopy **8,** 26 (1993).
21. G. M. Storry, C. Marcott, and I. Noda, Proc. SPIE, **2089,** 242 (1993).
22. E. Y. Jiang, R. A. Palmer, N. E. Ban-, and N. Morosoff, Appl. Spectrosc. **51,** 1238 (1997).
23. I. Noda, Appl. Spectrosc. **47,** 1329 (1993).
24. J. B. Huang and M. W. Urban, Appl. Spectrosc. **46,** 1666 (1992).
25. K. Ohta and H. Ishida, Appl. Spectrosc. **42,** 952 (1988).
26. G. K. Ribbegard and R. N. Jones, Appl. Spectrosc. **34,** 638 (1980).